Supporting Information

Reduced Auger Coefficient through Efficient Carrier Capture and Improved Radiative Efficiency from the Broadband Optical Cavity: A Mechanism for Potential Droop Mitigation in InGaN/GaN LEDs

Tarni Aggarwal[1], Ankit Udai[1], Pratim K. Saha[1], Swaroop Ganguly[1], Pallab Bhattacharya[2], and *Dipankar Saha[1]

[1]Applied Quantum Mechanics Laboratory, Indian Institute of Technology Bombay, Mumbai 400076, India. *Email: dipankarsaha@iitb.ac.in

[2]Solid-State Electronics Laboratory, Department of Electrical Engineering and Computer Science, University of Michigan, Ann Arbor, Michigan, 48109-2122, USA

S1. Sample preparation

Three sets of samples are prepared: 1) 8 DBR pairs on the frontside (F8), 2) 8 DBR pairs on the front and 5 pairs on the backside (F8B5), and 3) 8 pairs on the front and 10 pairs on the backside (F8B10), as depicted in **Figure S1**. The deposited DBR pairs consist of alternating layers of SiO_2 (refractive index, n_L=1.47) and HfO_2 (refractive index, n_H=2.15) with 45 and 85 nm thicknesses, respectively. Optical cavity formation can be observed with the ascending number of DBR pairs in F8, F8B5, and F8B10

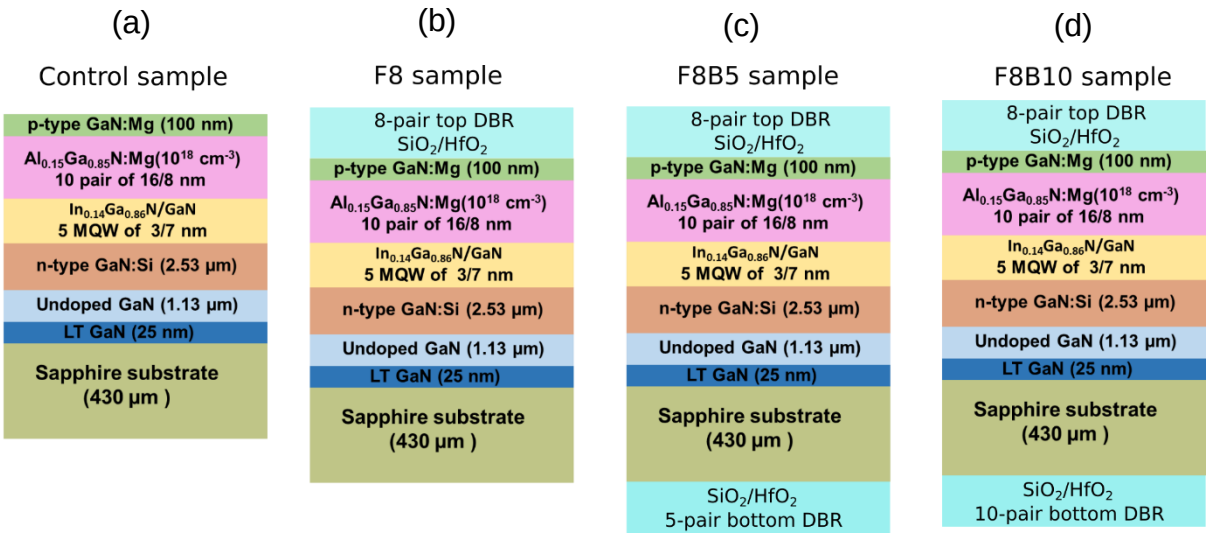

Figure S1: (a) Schematic of InGaN/GaN heterostructures (control sample), (b) 8 DBR pairs on the frontside (F8), (c) 8 DBR pairs on the front and 5 pairs on the backside (F8B5), and (d) 8 pairs on the front and 10 pairs on the backside (F8B10) sample**.**

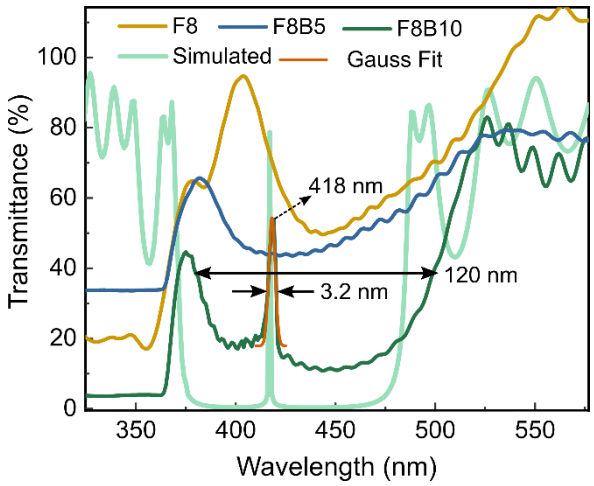

Figure S2: Transmission spectra of all the samples, cavity formation can be observed with the ascending number of DBR pairs in F8, F8B5, and F8B10 samples. A simulated transmission spectrum of the F8B10 sample is also depicted therein. The gaussian peak fitting is shown along with the obtained linewidth (~3.2 nm), and the wide stopband width (120 nm) are also highlighted.

samples. The central wavelength of the cavity formed in the F8B10 sample is at ~415 nm, and a ~120 nm wide broad stopband is formed with 20% transmittance. The simulated transmittance spectrum of the F8B10 sample is also shown therein, and it is in good agreement with the measurements.

The cavity in this work is different from the cavity typically used in GaN-based VCSELs. In our case, the bottom DBR is deposited below the sapphire substrate layer (as shown in **Figure S1(d)**). Therefore, cavity length is larger than that of the VCSEL cavity where the MQW active region is sandwiched between the top and bottom DBR layers[1–4]. As a result, we have a wide stopband of ~120 nm wide and the transmittance within the stopband in significantly greater than zero (~20%), as depicted in the transmittance spectra of F8B10 sample in **Figure S2**. In addition, the cavity mode which is at ~418 nm has a large linewidth of ~3.2 nm in contrast to the VCSELs where it is in the range of 1.5-0.5 nm[4]. We have now added this explanation in the updated manuscript.

S2. Details of Transient absorption spectroscopy setup

A pump pulse of 3.81 eV energy is used to excite the samples. Delayed weak broadband (350-800 nm) probe pulse, passing through the sample, carries the information on the excited-state dynamics. Change in absorption spectra of the probe

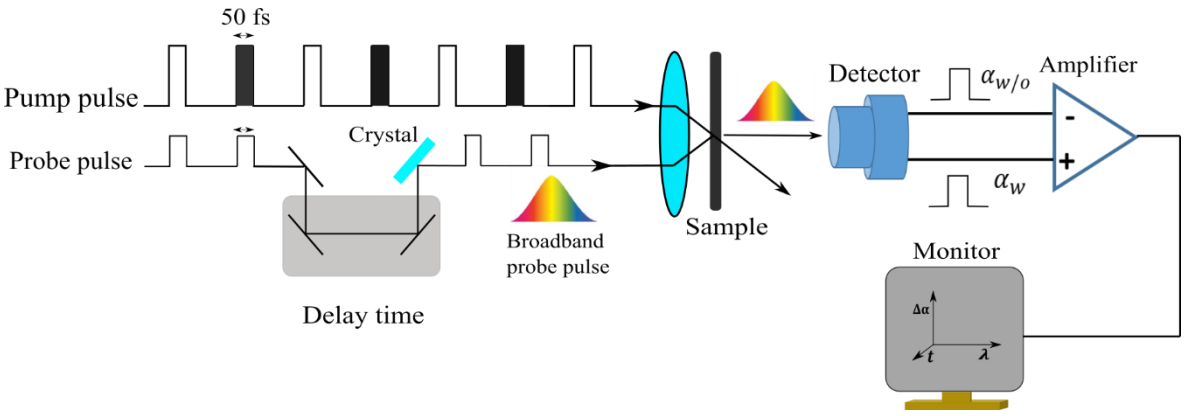

Figure S3 Basic block diagram and working principle of TAS setup.

pulse passing through an excited and non-excited sample is recorded at each time delay. Relative differential absorption $\Delta\alpha(\lambda, t)$ of the probe pulse is given as[5],

$$\Delta\alpha(\lambda, t) = \frac{\alpha_w(\lambda, t) - \alpha_{wo}(\lambda)}{\alpha_{wo}(\lambda)}$$

here, α_w and α_{wo} are the absorption coefficients of the probe pulse with and without pump-induced excitation, respectively.

S3. InGaN effective band-edge initial kinetics

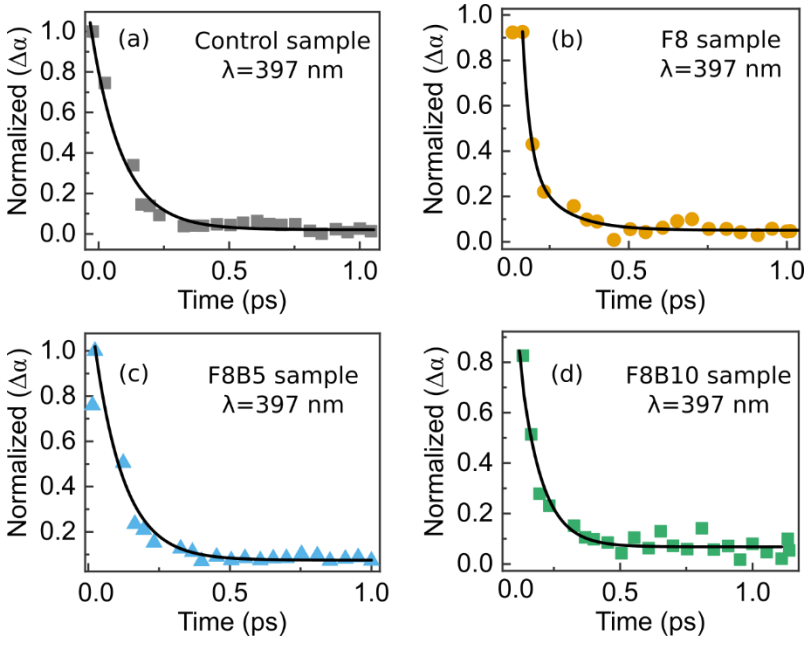

Figure S4 Single exponential fitting of capture kinetics at the InGaN band-edge of (a) Control sample, (b) F8 sample, (c) F8B5 sample, and (d) F8B10 sample.

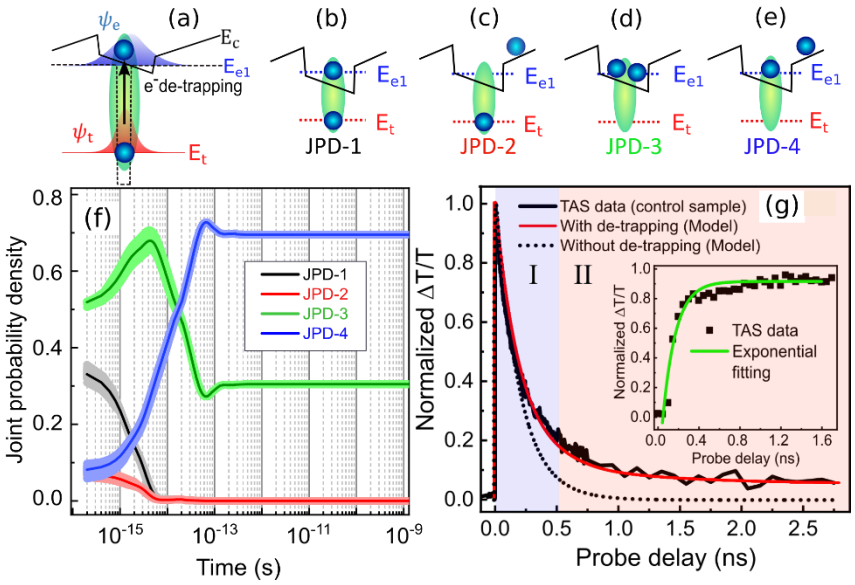

Figure S5 (a) Illustration of de-trapping mechanism; (b) to (e) are the schematic of JPDs; (f) time evolution of JPDs (g) carrier kinetics obtained from pump-probe spectroscopy, matching with the theoretical estimation from the modified rate equations is also shown.

S4: Electron de-trapping from the sub-bandgap states[6]

The carriers trapped in the sub-bandgap states do not necessarily recombine with the opposite charge carriers. Instead, the carrier can escape into the conduction band (CB) due to Coulombic interaction with those in the CB. **Figure S5(a)** depicts the carrier recovery in a quantum well system, where E_t is the trap energy level. The recovery mechanism is manifested experimentally by ultrafast pump-probe spectroscopy. A theoretical framework is also developed to obtain the probability of such transitions in InGaN/GaN quantum-confined heterostructures.

A two-particle Hamiltonian gives an adequate description of a system under Coulombic interaction. Here, one electron is in the nominal ground state (E_{e1}) in the QW, and the other electron is trapped in any of the sub-bandgap states (E_t). Electron-electron scattering due to screened Coulombic interaction serves as the perturbation in the system. The time-dependent joint probability density (JPD) is calculated by taking the projection of Fermionic wavefunction onto the original eigenstate. There are four probabilistic outcomes from the interaction of two electrons, listed as JPD1 to JPD4 in **Figure S5(b)** to **S5(e).**

Taking JPD3 and JPD4 into account, conventional rate equations are solved numerically, and excess carrier decay kinetics are obtained. **Figure S5(g)** shows the differential transmission data of a typical InGaN/GaN QW heterostructure obtained from femtosecond pump-probe spectroscopy. The kinetics correspond to the excess carrier decay after optical excitation. The matching of experimental data with the simulation model is shown in a solid red line. It is evident that the kinetics matches with the experimental data when quantum correction (JPD3 and JPD4) is taken into account.

S5. **Derivation of rate equation for Auger and BTB recombination.**

$$\frac{dn}{dt} = -C_\beta n^\beta$$

$$\int n^{-\beta} dn = -C_\beta \int dt$$

$$\left[\frac{n^{-(\beta-1)}}{-(\beta-1)}\right]_{n_o}^{n(t)} = -C_\beta [t]_0^t$$

$$\frac{\left[n(t)^{-(\beta-1)} - n_o^{-(\beta-1)}\right]}{-(\beta-1)} = -C_\beta t$$

$$\frac{n(t)^{-(\beta-1)}}{n_o^{-(\beta-1)}} - 1 = (\beta - 1\,) n_o^{(\beta-1)} C_\beta t$$

$$\left[\frac{n_o}{n(t)}\right]^{(\beta-1)} - 1 = (\beta - 1\,) n_o^{(\beta-1)} C_\beta$$

S6. Amplified spontaneous emission in F8B10 sample

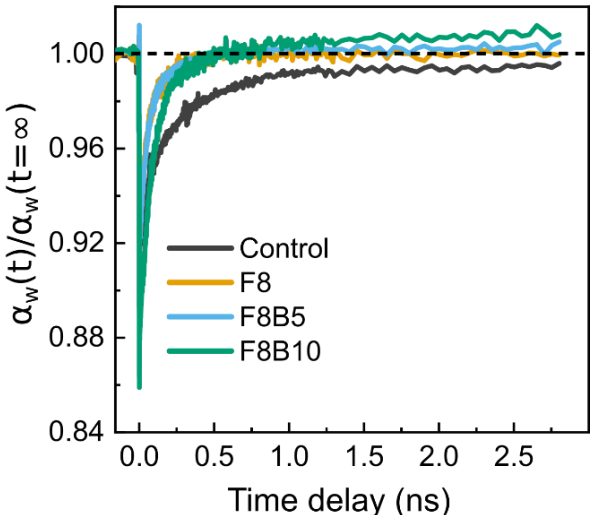

Figure S6 Normalized Differential absorption kinetics at the InGaN band-edge, of all the samples are depicted. Normalized $\Delta\alpha$ value greater than one in F8B10 sample, is the signature of ASE.

S7. Peak excess carrier density

The estimated peak excess carrier density in TAS measurements at different pump fluences are given below,

Pump fluence in TAS $(\mu J/cm^2)$	$n_o(cm^{-3}) = j\sigma/V$
820	3.18×10^{20}
715	2.77×10^{20}
500	1.94×10^{20}
450	1.74×10^{20}
360	1.30×10^{20}

S8. Theory of Auger recombination coefficient

We have also numerically calculated the Auger recombination coefficient as a function of polarization filed in the QW to corroborate our reasoning of suppressed Auger recombination in the presence of optical feedback. Direct Auger recombination

process involving three electron states (two electrons) in a conduction band and a heavy hole in the valence band (CCCH) is considered in our calculations for the InGaN/GaN QW system[7–9]. Figure 9a of the main manuscript depicts the E-k diagram with CCCH Auger recombination process, considering the ground states E_{e1} and E_{h1} for electrons and holes, respectively. As a result of electron-electron scattering originated from Coulombic interaction between electrons 1 and 2, recombination with a heavy-hole in the valence band (1') and transition of another electron to the higher state (2') takes place. The expression of total Auger recombination rate per unit volume in the QW structure is given as[7–9],

$$R = \frac{2\pi}{\hbar}\left(\frac{1}{4\pi}\right)^4 \frac{1}{L_z}\int \left|M_{if}\right|^2 P(1,1',2,2')\delta\left(E_i - E_f\right)\delta(k_1 + k_2 - k_{1'} - k_{2'})\, d^2k_1\, d^2k_2\, d^2k_{1'}\, d^2k_{2'}$$

here, L_z is the well width in growth direction (z-axis), $\left|M_{if}\right|^2$ is the square of matrix element, $P(1,1',2,2')$ corresponds to the occupation probability of the initial and final states in the process. Last two terms are the result of energy and momentum conservation during Coulombic scattering. Momentum transferred in the plane of the QW during electron-electron scattering is $k = (k_1 - k_{1'}) = (k_{2'} - k_2)$. Matrix element is calculated as,

$$M_{if} = \int\int [\phi_1^*(x_1)\phi_2^*(x_2) - \phi_2^*(x_1)\phi_1^*(x_2)] \times \left[\frac{e^2}{4\pi\epsilon|x_1 - x_2|}\exp(-\lambda|x_1 - x_2|)\right]\phi_{1'}(x_1)\phi_{2'}(x_2)\, dx_1\, dx_2$$

here, $\phi_1(x_1), \phi_2(x_2)$ are the initial wavefunction of electrons 1 and 2 and $\phi_{1'}(x_1), \phi_{2'}(x_2)$ are the final states, λ is the screening wavevector. The term $P(1,1',2,2')$ is given as,

$$P(1,1',2,2') = f_c(1)f_c(2)f_v(1')[1 - f_c(2')]\left[1 - exp\left(\frac{-E_t - E_{fc} - E_{fv}}{kT}\right)\right]$$

here, $f_c(1), f_c(2)$ are the occupation probability of initial states and $f_v(1')$, $[1 - f_c(2')]$ are the occupation-probability of final states. E_t is the minimum kinetic energy required

for $2'$ electron, in order to satisfy momentum energy conservation. E_{fc} and E_{fv} are the quasi-Fermi levels for the conduction and the valence band, respectively.

References

(1) Yu, H.; Zheng, Z.; Mei, Y.; Xu, R.; Liu, J.; Yang, H.; Zhang, B.; Lu, T.; Kuo, H. Progress and Prospects of GaN-Based VCSEL from near UV to Green Emission. *Progress in Quantum Electronics* **2018**, *57*, 1–19. https://doi.org/10.1016/j.pquantelec.2018.02.001.

(2) Khreis, O. M. Modeling and Analysis of Smoothly Diffused Vertical Cavity Surface Emitting Lasers. *Computational Condensed Matter* **2016**, *9*, 56–61. https://doi.org/10.1016/j.cocom.2016.09.005.

(3) Okur, S.; Shimada, R.; Zhang, F.; Hafiz, S. D. A.; Lee, J.; Avrutin, V.; Morkoç, H.; Franke, A.; Bertram, F.; Christen, J.; et al. GaN-Based Vertical Cavities with All Dielectric Reflectors by Epitaxial Lateral Overgrowth. *Japanese Journal of Applied Physics* **2013**, *52* (8S), 08JH03. https://doi.org/10.7567/JJAP.52.08JH03.

(4) Butté, R.; Feltin, E.; Dorsaz, J.; Christmann, G.; Carlin, J.-F.; Grandjean, N.; Ilegems, M. Recent Progress in the Growth of Highly Reflective Nitride-Based Distributed Bragg Reflectors and Their Use in Microcavities. *Japanese Journal of Applied Physics* **2005**, *44* (10), 7207–7216. https://doi.org/10.1143/JJAP.44.7207.

(5) Aggarwal, T.; Udai, A.; Banerjee, D.; Pendem, V.; Chouksey, S.; Saha, P.; Sankaranarayanan, S.; Ganguly, S.; Bhattacharya, P.; Saha, D. Investigation of Ultrafast Carrier Dynamics in InGaN/GaN-based Nanostructures Using Femtosecond Pump-Probe Absorption Spectroscopy. *physica status solidi (b)* **2021**, *51* (Supplement), pssb.202100223. https://doi.org/10.1002/pssb.202100223.

(6) Aggarwal, T.; Ganguly, S.; Saha, D. Carrier Recovery from Sub-Bandgap States in a Gan-Based Quantum-Confined Structure: Identification of Carrier Reservoirs through Femtosecond Pump-Probe Spectroscopy. *Journal of Physical Chemistry C* **2021**, *125* (6), 3535–3541. https://doi.org/10.1021/acs.jpcc.0c09892.

(7) Delaney, K. T.; Rinke, P.; Van de Walle, C. G. Auger Recombination Rates in Nitrides from First Principles. *Applied Physics Letters* **2009**, *94* (19), 191109. https://doi.org/10.1063/1.3133359.

(8) Kioupakis, E.; Yan, Q.; Steiauf, D.; Van de Walle, C. G. Temperature and Carrier-Density Dependence of Auger and Radiative Recombination in Nitride Optoelectronic Devices. *New Journal of Physics* **2013**, *15* (12), 125006. https://doi.org/10.1088/1367-2630/15/12/125006.

(9) Dutta, N. K. Calculation of Auger Rates in a Quantum Well Structure and Its Application to InGaAsP Quantum Well Lasers. *Journal of Applied Physics* **1983**, *54* (3), 1236–1245. https://doi.org/10.1063/1.332185.